

Irregularity of the Magnetic Island Rotation under External Helical Magnetic Perturbation in T-10 Tokamak

N.V. Ivanov, A.M. Kakurin, I.I. Orlovskiy
Nuclear Fusion Institute, RRC «Kurchatov Institute», Moscow, Russia

Introduction

The T-10 tokamak experimental observations of the $m = 2$ mode rotation irregularity is analysed in the course of development of a method of the error field identification. It is supposed that the observed variations of the tearing mode rotation velocity [1 – 3], which take place along with the magnetic island rotation, can be attributed to the effect of the External Helical Magnetic Perturbation (EHMP) of the same helicity. The experimental results are simulated using a rotation model for the non-linear Rutherford tearing mode [4, 5]. The rotation velocity of the mode is represented by a superposition of the velocity of the mode with respect to the plasma that arises as a characteristic of an externally driven non-linear tearing mode and the plasma rotation velocity affected by the plasma interaction with the external magnetic perturbation.

Experimental Arrangement and Processing of the MHD Data

T-10 is a tokamak with a circular plasma cross-section. The major and minor radii of the vacuum vessel are $R = 1.5$ m and $b = 0.42$ m, the radius of the permanent circular limiter is 0.33 m. The experiments were carried out at the discharge parameters: toroidal magnetic field $B_T = 2.4$ T, discharge current $I_p = 240$ kA, line-average plasma density $n_e = (7-8) \cdot 10^{19} \text{ m}^{-3}$. The plasma minor radius determined by the position of a movable rail limiter was $a = 0.27$ m. In our experiment the EHMP consisted of a superposition of the permanent error field, artificially applied magnetic field of the halo-current introduced into the SOL plasma as described in [6, 7] and a magnetic field of eddy currents in the vacuum vessel wall. The $m = 2, n = 1$ harmonic of EHMP produced by the 100 A halo-current can be estimated as 10^{-4} T at the plasma boundary.

The space structure of the MHD mode is measured with a set of poloidal magnetic field sensors located at the inner side of the vacuum vessel wall. The observed $m = 2$ mode rotation irregularity has a time-scale comparable with the period of the oscillations. In this case instead of the standard spectral processing of the MHD signals we calculate the instantaneous value of the mode frequency as the time derivative of the spatial phase of the magnetic perturbation. The procedure includes a decomposition of the measured magnetic perturbation to a set of spatial Fourier harmonics with different poloidal and toroidal numbers. For each harmonic with certain m and n numbers the poloidal magnetic field perturbation at the radial position of the magnetic sensors is

$B_\theta(\theta, \varphi, t) = B_{\theta C}(t)\cos(m\theta + n\varphi) + B_{\theta S}(t)\sin(m\theta + n\varphi)$, where φ and θ are the toroidal and poloidal angles, $B_{\theta C}(t)$ and $B_{\theta S}(t)$ are the cosine and sine components of the measured harmonic of the magnetic perturbation. The space amplitude of the harmonic is $\text{Ampl } B_\theta(t) = \sqrt{B_{\theta C}^2(t) + B_{\theta S}^2(t)}$. The space phase of this harmonic is defined as $\Phi(t) = \text{arctg}[B_{\theta S}(t)/B_{\theta C}(t)]$ and the instantaneous value of the mode frequency is $\Omega(t) = d\Phi/dt$.

Experimental Observations

The experimental waveforms of the halo-current and the $m = 2$ mode signals are shown in Fig.1 for cases of different halo-current directions and amplitudes. The dependencies on the halo-current of the maximum and minimum values of the mode instantaneous frequency over the oscillation period are shown in Fig.2. In Fig.1 and Fig.2, one can see that the halo-current affects the instantaneous value of

the mode rotation frequency. The mode rotation stops in cases of high amplitude halo-current pulses. This effect has different threshold values at the negative and positive halo-current directions. In cases of moderate halo-current amplitude, the effect on the mode rotation depends on the halo-current direction. The negative halo-current causes an increase of the mode oscillation frequency, the oscillations become more regular. In case of the positive halo-current pulse, the application of the halo-current is followed by a decrease of the mode frequency and a rise of the rotation irregularity. We attribute the observed changes of the mode oscillations to the joint effect of the permanent error field and the magnetic field of the applied halo-current. In the case of the negative J_{HALO} , a partial compensation of the error field by the halo-current field takes place. Under this assumption, we estimate the amplitude of $m = 2$, $n = 1$ harmonic of the error field from the horizontal asymmetry of the dependencies in Fig.2. The EHMP corresponding to (100–200) A horizontal shift of these dependencies along the J_{HALO} axis can be estimated as $(1-2) \cdot 10^{-4}$ T, that is $(4-8) \cdot 10^{-5} B_T$.

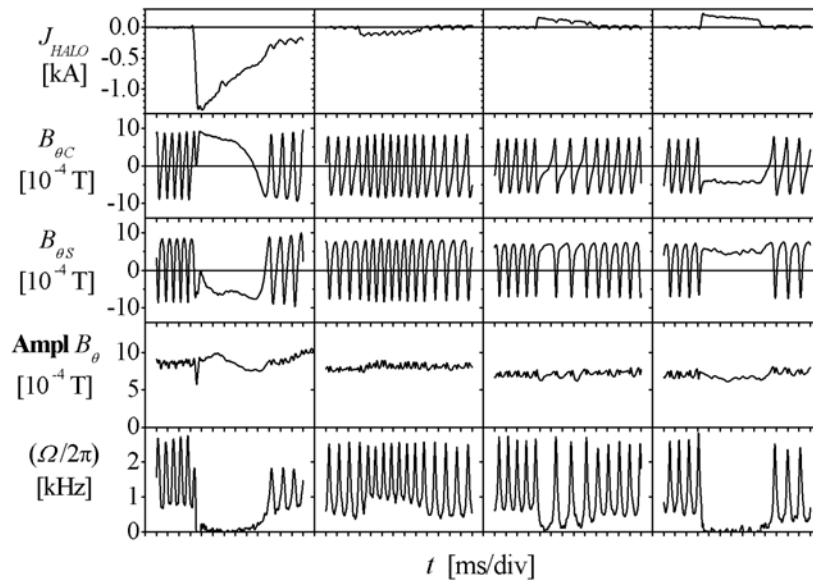


Fig.1. Waveforms of the halo-current, J_{HALO} , the $m = 2$ mode cosine, B_C , and sine, B_S , space components, space amplitude, $\mathbf{Ampl} B_\theta$, and instantaneous value of the mode frequency, Ω

the mode rotation frequency. The mode rotation stops in cases of high amplitude halo-current pulses. This effect has different threshold values at the negative and positive halo-current directions. In cases of moderate halo-current amplitude, the effect on the mode rotation depends on the halo-current direction. The negative halo-current causes an increase of the mode oscillation frequency, the oscillations become more regular. In case of the positive halo-current pulse, the application of the halo-current is followed by a decrease of the mode frequency and a rise of the rotation irregularity. We attribute the observed changes of the mode oscillations to the joint effect of the permanent error field and the magnetic field of the applied halo-current. In the case of the negative J_{HALO} , a partial compensation of the error field by the halo-current field takes place. Under this assumption, we estimate the amplitude of $m = 2$, $n = 1$ harmonic of the error field from the horizontal asymmetry of the dependencies in Fig.2. The EHMP corresponding to (100–200) A horizontal shift of these dependencies along the J_{HALO} axis can be estimated as $(1-2) \cdot 10^{-4}$ T, that is $(4-8) \cdot 10^{-5} B_T$.

the mode rotation frequency. The mode rotation stops in cases of high amplitude halo-current pulses. This effect has different threshold values at the negative and positive halo-current directions. In cases of moderate halo-current amplitude, the effect on the mode rotation depends on the halo-current direction. The negative halo-current causes an increase of the mode oscillation frequency, the oscillations become more regular. In case of the positive halo-current pulse, the application of the halo-current is followed by a decrease of the mode frequency and a rise of the rotation irregularity. We attribute the observed changes of the mode oscillations to the joint effect of the permanent error field and the magnetic field of the applied halo-current. In the case of the negative J_{HALO} , a partial compensation of the error field by the halo-current field takes place. Under this assumption, we estimate the amplitude of $m = 2$, $n = 1$ harmonic of the error field from the horizontal asymmetry of the dependencies in Fig.2. The EHMP corresponding to (100–200) A horizontal shift of these dependencies along the J_{HALO} axis can be estimated as $(1-2) \cdot 10^{-4}$ T, that is $(4-8) \cdot 10^{-5} B_T$.

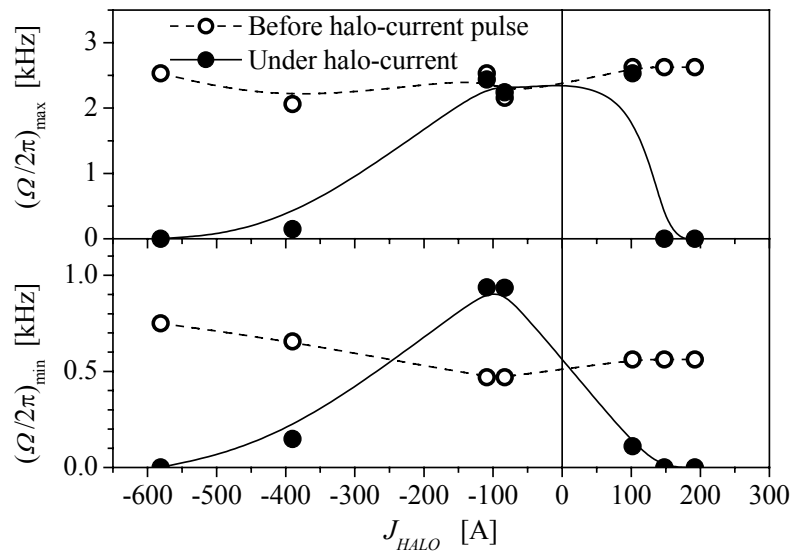


Fig.2. Dependencies of maximum and minimum values of the mode instantaneous frequency on the applied halo-current

Numerical Modelling

As in [6, 7], the non-linear tearing mode rotation in presence of the EHMP of the same poloidal, m , and toroidal, n , numbers is simulated in cylindrical approximation using the Rutherford model [4, 5]. We assume that the external magnetic field is produced by three current layers at radii $r = r_l$ outside the plasma. The equations

$$\frac{\partial}{\partial r} \left(r \frac{\partial \Psi_{C,S}}{\partial r} \right) - \left(\frac{m^2}{r} + \frac{\mu_0 R}{B_T} \frac{\partial i / \partial r}{\mu(r) - n/m} \right) \Psi_{C,S} = \mu_0 \sum_l r j_{l,C,S} \delta(r - r_l) \quad (1), (2)$$

are used for the calculation of the radial distribution of the cosine, Ψ_C , and sine, Ψ_S , components of the poloidal magnetic flux perturbation, $\Psi = \Psi_C(r, t) \cos(m\theta + n\varphi) + \Psi_S(r, t) \sin(m\theta + n\varphi)$, satisfying $B_\theta = -\partial \Psi / \partial r$, $B_r = (1/r) \partial \Psi / \partial \theta$ and the boundary conditions $\Psi_{C,S}(0) = \Psi_{C,S}(\infty) = 0$. In (1) and (2), $i(r)$ is the plasma current density, $\mu(r) = I/q(r)$, $\mu_0 = 4\pi \cdot 10^{-7}$ [H/m], j_{lC} and j_{lS} are the cosine and sine components of the external helical current surface densities at radii $r = r_l$: $j_l = j_{lC}(t) \cos(m\theta + n\varphi) + j_{lS}(t) \sin(m\theta + n\varphi)$, including the current which produces the error field, the halo-current at $r = a$ and the current with the surface density, $j_{bC,S} = -\zeta \sigma \frac{d\Psi_{C,S}(r_b)}{dt}$, generated in the resistive vacuum vessel wall at $r = b$ due to magnetic flux variations in time. In the $j_{bC,S}$ formula, ζ is the thickness of the vacuum vessel wall and σ is the wall conductivity. The time evolution of the cosine and sine components of the magnetic flux perturbation at $r = r_s$ is described by the equations:

$$\frac{d\Psi_C}{dt} = \pi a^2 \omega_R \frac{\Delta'_C(W)}{W} \Psi_C - \Omega_0 \Psi_S, \quad (3)$$

$$\frac{d\Psi_S}{dt} = \pi a^2 \omega_R \frac{\Delta'_S(W)}{W} \Psi_S + \Omega_0 \Psi_C. \quad (4)$$

In (3) and (4), $\omega_R = 1/\tau_R$, $\tau_R = \mu_0 a^2/\eta$ is the resistive time. The right-hand sides of the equations (3) and (4) are expressed through stability parameters for cosine and sine components of the magnetic flux perturbation:

$$\Delta'_{C,S} = \frac{\Psi'_{C,S}(r_s + W/2) - \Psi'_{C,S}(r_s - W/2)}{\Psi_{C,S}(r_s)}, \quad \text{where } W = 4 \sqrt{\frac{R \sqrt{\Psi_C^2 + \Psi_S^2}}{r_s B_T d\mu/dr}} \Big|_{r_s}$$

magnetic island. In (3) and (4), the natural frequency, $\Omega_0 = m \frac{v_\theta}{r_s} + n \frac{v_\varphi}{R}$, is a free parameter

depending on the toroidal, v_φ , and poloidal, v_θ , rotation velocities of the resonant plasma layer in the vicinity of the resonant magnetic surface. Similar to [8-10], we use the equations of angular motion in the toroidal and poloidal directions to calculate the time variations of these velocities. We assume that the plasma inertia in the resonant plasma layer, $r_s - W/2 \leq r \leq r_s + W/2$, is balanced by the sum of the electromagnetic and viscous friction forces. The electromagnetic force is calculated as a reaction to the force applied to the conductors with the external helical currents from the magnetic field perturbation originated by the tearing mode. The toroidal and poloidal components of the force moment

applied to the resonant plasma layer are: $M_\varphi = -\frac{n}{m} \sum_l r_l \int_{S_l} j_l B_r dS$, $M_\theta = -\sum_l r_l \int_{S_l} j_l B_r dS$,

where the integration is performed over the surfaces, S_l , corresponding to the external current layers at radii, $r = r_l$, we assume that $R \gg a$, $m \geq n$. The angular motion equations for the resonant layer in the toroidal and poloidal directions are:

$$\frac{I_\varphi}{R} \frac{dv_\varphi}{dt} = M_\varphi - M_{FR\varphi} - \frac{v_\varphi - v_{\varphi 0}}{R} \frac{dI_\varphi}{dt}, \tag{5}$$

$$\frac{I_\theta}{r_s} \frac{dv_\theta}{dt} = M_\theta - M_{FR\theta} - \frac{v_\theta - v_{\theta 0}}{r_s} \frac{dI_\theta}{dt}. \tag{6}$$

In the equations (5) and (6), I_φ and I_θ are the toroidal and poloidal inertial moments of the resonant plasma layer which can be evaluated as $I_\varphi = 4\pi^2 R^3 r_s W \rho$, $I_\theta = 4\pi^2 R r_s^3 W \rho$,

where ρ is the plasma specific mass, $M_{FR\varphi,\theta}$ are the toroidal and poloidal moments of the viscous friction force, which are supposed to be proportional to the differences between $v_{\varphi,\theta}$ and the components of the plasma intrinsic rotation velocity, $v_{0\varphi,\theta}$, outside the resonant plasma layer.

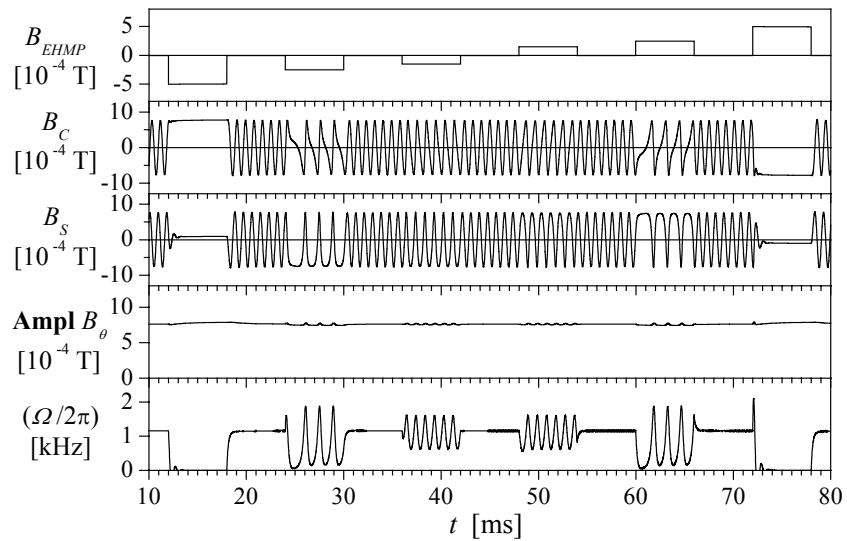


Fig.3. The calculated effect of the EHMP on the mode rotation

The result of the simulation is shown in Fig.3. Similar to the experiment, the irregularity of the mode rotation takes place at EHMP of both directions in case of the EHMP absolute value lower than necessary for the complete mode locking.

Acknowledgements

We would like to thank V.D.Pustovitov for helpful discussions. This work is supported by the Atomic Energy Agency of the Russian Federation.

References

1. Volkov, V.V., Ivanov, N.V., Kakurin, A.M. et al. 22nd EPS Conference on Controlled Fusion and Plasma Physics. Bournemouth 1995. Contributed papers III-077. Volkov, V.V., Ivanov, N.V., Kakurin, A.M. et al. Plasma Phys. Rep. **21** (1995) 881.
2. D.A. Gates, T.C. Hender. Nucl. Fusion, **36** (1996) 273.
3. Craven, W.A., Wootton, A.J., Nucl. Fusion **38** (1998) 585.
4. Rutherford, P.H., Phys. Fluids **16** (1973) 1903.
5. White, R.B., Monticello, D.A., Rosenbluth, M.N., Waddell, B.V., Phys. Fluids **20**, (1977) 800.
6. Chudnovskiy, A.N., Gvozdkov, Yu.V., Ivanov, N.V. et al. Nucl. Fusion, **43** (2003) 681.
7. Chudnovskiy, A.N., Ivanov, N.V., Kakurin A.M. et al. Nucl. Fusion, **44** (2004) 287.
8. Nave, M.F.F., Wesson, J.A., Nucl. Fusion, **30** (1990) 2575.
9. Fitzpatrick, R., Nucl. Fusion, **33** (1993) 1049.
10. Fitzpatrick, R., Phys. Plasmas, **5** (1998) 3325.